PHOTOCONDUCTIVITY AND LIGHT INDUCED PHENOMENA IN AMORPHOUS $(As_4S_3Se_3)_{1-x}$:Sn_x THIN FILMS

O. V. Iaseniuc, M. S. Iovu, I. A. Cojocaru, and A. M. Prisacar

Institute of Applied Physics, Academy of Sciences of Moldova,
str. Academiei 5, Chisinau, MD-28 Republic of Moldova
E-mail: oxana.iaseniuc@phys.asm.md

(Received May 05, 2014)

Abstract

Amorphous arsenic trisulfide (As_2S_3) and arsenic triselenide (As_2Se_3) are widely investigated amorphous materials due to their interesting electrical, optical, and photoelectrical properties. Mixed amorphous materials, such as (As_2S_3):(As_2Se_3), are of special interest for improving the physical properties and recording characteristics and extending the spectral range of photosensibility. Chalcogenide vitreous semiconductors (ChVSs) of the As-S-Se system exhibit photostructural transformations with reversible and irreversible properties and are promising materials as registration media for holography and optical information, for fabrication of diffractive elements, and other optoelectronic applications. Because many optoelectronic devices on amorphous semiconductors are based on the photoconductivity effect, it is of particular interest to study the steady-state and transient characteristics of photoconductivity. In this paper, experimental results for steady-state photoconductivity and holographic characteristics of amorphous $(As_4S_3Se_3)_{1-x}$:Sn_x thin films are described. It was shown that the photoconductivity spectra depend on the polarity on the top illuminated electrode and on the Sn concentration in the host glass. The photosensitivity of amorphous $(As_4S_3Se_3)_{1-x}$:Sn_x thin films is almost constant for all Sn-containing glasses. The Moss rule was used for determination of optical forbidden gap E_g from the photoconductivity spectra. It was demonstrated that the investigated amorphous films are sensitive to light irradiation and can be used as effective registration media for holographic information. The relaxation of photodarkening in amorphous $(As_4S_3Se_3)_{1-x}$:Sn_x thin films was investigated; it was shown that the relaxation curves of transmittance $T/T_0 = f(t)$ can be described by stretch exponential function $T(t)/T(0) = A_0 + A\exp[-(t-t_0)/\tau]^{(1-\beta)}$. The kinetics of diffraction efficiency growth $\eta(t)$ was measured by registration of the laser intensity of the 1st interference maximum versus time exposure. With an increase in the Sn concentration in amorphous $(As_4S_3Se_3)_{1-x}$:Sn_x thin films up to 6.0 at % Sn, diffraction efficiency η increases; at higher tin concentrations, it decreases.

1. Introduction

Photoconductivity represents a change in conductivity under the action of light radiation. Photoconductivity spectra can provide information about the generation, drift, and recombination of nonequilibrium current carriers [1]. In our previous works, some physical and optical properties of amorphous $(As_4S_3Se_3)_{1-x}$:Sn_x thin films have been described [2, 3]. Chalcogenide vitreous semiconductors (ChVSs) of the As-S-Se system exhibit photostructural transformations with reversible and irreversible properties and are promising materials as registration media for

holography and optical information, for fabrication of diffractive elements, and other optoelectronic applications [4, 5]. Because many optoelectronic devices on amorphous semiconductors are based on the photoconductivity effect, it is of particular interest to study the steady-state and transient characteristics of photoconductivity. Evaporated amorphous thin films are shown to have a high degree of structural disorder depending on the composition and foreign impurities. The electrical, optical, and photoelectrical properties of chalcogenide glasses can be varied and regulated over an extensive range by modifying the composition and production technique. It was shown that the addition of a Sn impurity in amorphous As_2S_3 and AsSe thin films can provide a pronounced effect on the electrical and transport properties and optical and photoinduced phenomena [6-10]. In the last years, special attention has been paid to the influence on the photostructural transformation in amorphous thin films doped with metal impurity. It has been shown that a Sn impurity introduced in the As_2Se_3, AsSe and Sb_2S_3 glass network reduce the photodarkening effect. According to ^{119}Sn Mössbauer spectroscopy, in the As_2Se_3:Sn_x glassy system, new tetrahedral $Sn(Se_{1/2})_4$ and quasi-octahedral SnSe structural units can be formed and influence the photostructural transformations. A decrease in the optical gap of As_2Se_3 glass upon Sn alloying, most likely, results from a broadening of the valence band, the top of which is formed by Se lone-pair electrons. It was demonstrated that tin impurities has a strong effect on transient rather than on steady-state photoconductivity. The enhanced deep trapping in doped As_2Se_3 delays the recombination process and slows down the initial photocurrent relaxation. The features of transient photoconductivity were found to be primarily controlled by deep carrier trapping with the energy distribution and concentration of deep traps being determined by the structure and composition of doped amorphous films [8]. In this paper, experimental results of steady-state photoconductivity, photodarkening relaxation and holographic characteristics of amorphous $(As_4S_3Se_3)_{1-x}$:Sn_x thin films are described. The photoconductivity spectra are used to determine some optical parameters.

2. Experimental

The bulk $(As_4S_3Se_3)_{1-x}$:Sn_x chalcogenide glasses (x = 0–10.0 at % Sn) were prepared from the elements of high purity 6N (As, S, Se, Sn) by the conventional melt quenching method. Thin film samples with thickness L = 0.5–17.5 μm were prepared by flash thermal evaporation in a vacuum (P = 10^{-5} Torr) of the synthesized initial glass onto glass substrates held at T_{substr} = 100°C. The thin film samples had a sandwich configuration with two Al electrodes; the top electrode was transparent for the incident light. In all the cases, measurement of dark conductivity σ_d and photoconductivity σ_{ph} for amorphous semiconductors with the low conductivity was performed at a constant current, e.g., the case of low load resistance $R_L \angle\angle R_d R_{ph}$, where R_L is the load resistance, R_d the sample resistance in the dark, and R_{ph} is the sample resistance under illumination. Forasmuch as the calibrated resistance of an U5-11 electrometrical amplifier was used as a load resistance, the error of the measurements was determined by the scatter of load resistance R_L; it was less than 1.0 %. Specific conductivity σ_S of the sample was calculated according to the expression

$$\sigma_S = \frac{1}{R_S} \cdot \frac{L}{S} = \frac{U_L}{U - U_L} \cdot \frac{1}{R_L} \cdot \frac{L}{S} \qquad (1)$$

Here, R_S is the resistance of the sample, S is the area between the electrodes of the sample, U is the total voltage in the electrical circuit, and U_L is the voltage on load resistance R_L

In order to initiate the photostructural transformations in the thin film samples a red (λ = 633 nm, P = 0.6 mW) and green (λ = 543 nm, P = 0.75 mW) continuous He−Ne lasers were used simultaneously as sources of light exposure. The relaxation of the transmission curves was measured both at λ = 633 nm and λ = 543 nm wavelengths in-situ during the light excitation. The experimental set-up included a laser and a PCI-1713A digital build-in PC-card for data acquisition connected to a Si-photodetector. Special software was elaborated for automatic measurements. The microholograms in the amorphous thin films were registered by means of the interference of two Ar^+-laser beams (λ = 0.488 μm) with a power of W = 0.64 mW. The kinetics of diffraction efficiency growth $\eta(t)$ was measured by registration of the intensity of the 1st interference maximum versus time exposure at wavelength λ = 0.6328 μm. Diffraction efficiency η was calculated as a ratio of the intensity in the 1st diffraction maximum to the intensity of the transmitted laser beam across the sample.

3. Experimental results and discussion

The photoconductivity spectra can give the information regarding the processes of generation, drift and recombination of non-equilibrium current carriers. The photoconductivity, which is determined as an increase in conductivity under light illumination, can be defined by the expression

$$\sigma_{ph} = \frac{1}{L} e\mu_d \tau \beta N_0 [1 - \exp(-kL)] \tag{2}$$

Here, N_0 is the number of incident photons on the sample surface per second, L is the thickness of the sample, β describes the efficiency of the generation process μ_d is the drift mobility of the holes, τ is the recombination life time, e is the electron charge, and k is the absorption coefficient. The exponential term describes the light absorption in the sample of the investigated material and thickness.

Figure 1 shows the spectral distribution of photocurrent for amorphous $(As_4S_3Se_3)_{0.97}$:$Sn_{0.03}$ thin films at positive (curve *1*) and negative (curve *2*) polarities at the top illuminated electrode. For other $(As_4S_3Se_3)_{1-x}$:Sn_x ($0 \le x \le 10$ at % Sn), the shape of the curves of the spectral distribution of photocurrent is similar. In all cases, the photocurrent at positive polarity at the top illuminated electrode is higher and the maximum of the spectral distribution is shifted in the high energy region of the spectrum (Fig. 2). Since the investigated spectral region ($h\nu$ = (0.95–3.1 eV) corresponds to the region of the optical absorption edge and the values of absorption coefficient k change four- to fivefold in this region, the spectral distribution of photoconductivity is analyzed in the approximation of strong and weak absorption.

In the region of strong absorption $\exp(-kL) \angle\angle 1$, the light is absorbed near the surface of the sample and photoconductivity is determined by the expression

$$\sigma_{ph} = \frac{1}{L} \cdot e\mu_d \tau \beta N_0 . \tag{3}$$

In this region of energy of the incident photons in the absence of strong surface recombination, the photoconductivity weakly depends of the photon energy, which gives the possibility to determine the product $\beta\mu_d\tau$ and which is characteristic of the photosensibility of the investigated semiconductor material.

In the approximation of weak absorption, at $\exp(kL) \approx 1 - kL$, from expression (1) we

obtain

$$\sigma_{ph} = e\mu_d \tau \beta k N_0 . \quad (4)$$

Relation (4) suggests that, in the region of weak absorption, the dependence of the spectral dependence of photoconductivity vs. energy of incident photons is determined by the spectral distribution of absorption coefficient k because, in this region, the product $\beta\mu_d\tau$ very weakly depends on photon energy [11]. This gives the possibility to use the photoconductivity spectra for calculating the optical absorption spectra in this region.

The low energy portion of the $log(I_{ph}/N_0)$ dependence is described by the Urbach tail of absorption coefficient α. The Moss rule was used for determining the optical forbidden gap E_g from the photoconductivity spectra. Usually, in chalcogenide glasses, the absorption edge is broader than in crystalline analogues, which is caused by a broad energy distribution of electronic states in the band gap due to disorder and defects. The distribution of the localized states of the semiconductor, including band gap E_g depend on the structure of the investigated material. A well-known tool for determining the band gap of the semiconductor is long wavelength λ_0 at which the photosensitivity achieves half maximum, as is shown in Fig. 1. The dependence of the calculated values of E_g^+ versus Sn concentration in amorphous $(As_4S_3Se_3)_{1-x}$:Sn_x thin films is shown in Fig. 2 (right Y axis). This dependence has a minimum at about 6.0 at % Sn, which is probably attributed to the formation of new tetrahedral units $SnSe_2$.

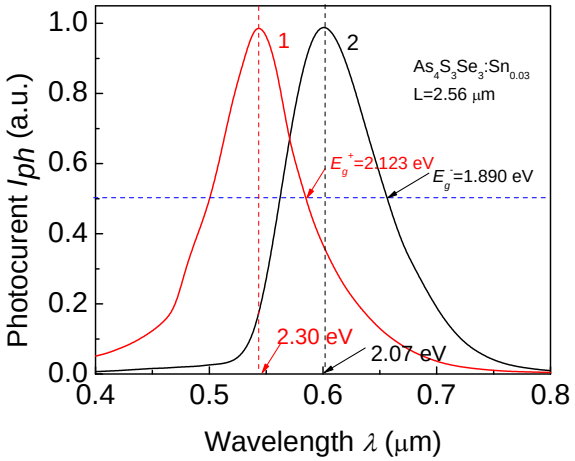

Fig. 1. Spectral distribution of photocurrent $I_{ph} = f(\lambda)$ for amorphous $(As_4S_3Se_3)_{0.97}$:$Sn_{0.03}$ thin films.

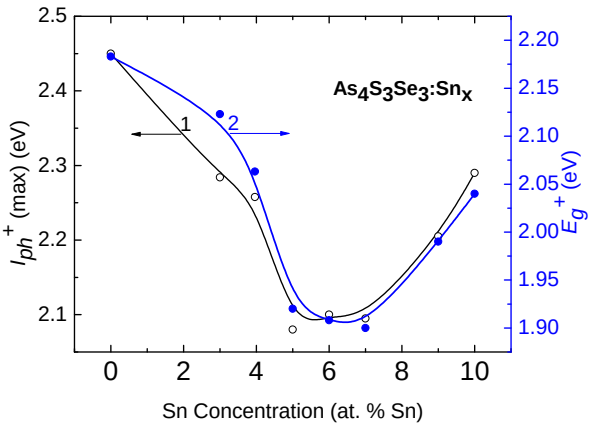

Fig. 2. Dependence of the maximum of the photocurrent $I_{ph}^+(max)$ and forbidden gap E_g^+ versus Sn concentration in amorphous $(As_4S_3Se_3)_{1-x}$:Sn_x thin films.

Figure 2 shows that the photocurrent is higher for the positive polarity on the illuminated top electrode and the maximum in the spectral distribution of photocurrent is displaced in the higher region of photon energy. At the negative polarity on the top illuminated electrode, the photocurrent decrease after the maximum. That is caused by the existence of a high concentration of recombination centers at the surface of the sample due to the presence of a lot of structural defects. For this reason, we can assume that the nonequilibrium carriers reaching the surface can be captured by the local centers and the recombination process is faster than in the bulk of the sample. The probability that the non-equilibrium carriers reach the surface is greater for the case where the incident light is absorbed in the small layer, e.g., at high absorption coefficients. For

this reason, we observe the fall of the photosensitivity in high energy region because, in the shot wavelength region, the absorption coefficient increases and the number of localized states involved in the optical transitions also increases.

Figure 3 shows the spectral distribution of photocurrent for some compositions of amorphous $(As_4S_3Se_3)_{1-x}$:Sn_x thin films. With an increase in the Sn concentration in amorphous $(As_4S_3Se_3)_{1-x}$:Sn_x thin films, the maximum of photocurrent $I_{ph}(max)$ and the values of optical band gap E_g are shifted to lower energies up to x = 6.0 at % Sn and, for higher concentrations, increase due to the formation of new tetrahedral structural units. The photosensitivity of amorphous $(As_4S_3Se_3)_{1-x}$:Sn_x thin films decreases upon the introduction of Sn into the host glass and is almost constant for all Sn-containing glasses. Figure 4 shows the normalized curves of the spectral distribution of photocurrent $log(I_{ph}/N_0) = f(h\nu)$ for amorphous $As_4S_3Se_3$ thin films. The same dependences are exhibited by all amorphous $(As_4S_3Se_3)_{1-x}$:Sn_x thin films with the different investigated compositions.

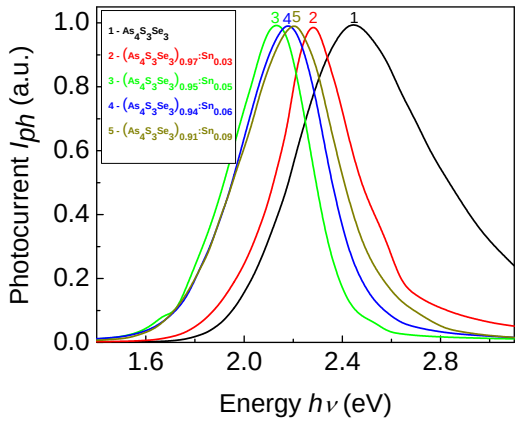

Fig. 3. Spectral distribution of photocurrent $I_{ph} = f(\lambda)$ for amorphous $(As_4S_3Se_3)_{1-x}$:Sn_x thin films.

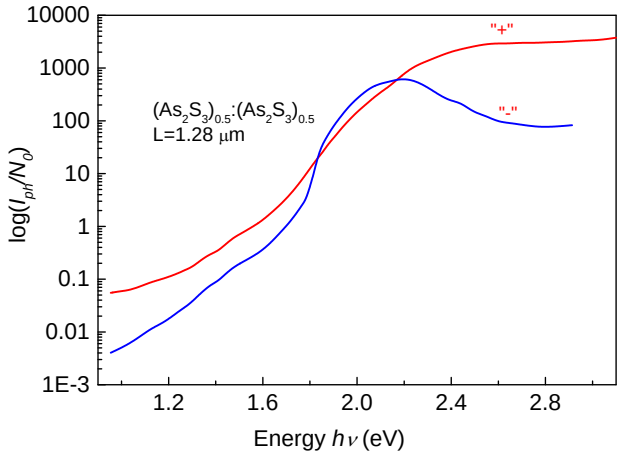

Fig. 4. Normalized curves of the spectral distribution of photocurrent $log(I_{ph}/N_0) = f(h\nu)$ for amorphous $As_4S_3Se_3$ thin films.

The amorphous $(As_4S_3Se_3)_{1-x}$:Sn_x thin films exhibit photoinduced effects under light irradiation with photon energy above the optical band gap ($h\nu \geq E_g$),which makes them promising materials for registration of optical and holographic information [2].

The relaxation of relative optical transmission $T/T_0 = f(t)$ under light exposure at wavelength λ = 633 nm and λ = 543 n for amorphous $(As_4S_3Se_3)_{1-x}$:Sn_x thin films is shown in Figs. 5 and 6, respectively.

At a constant light intensity, these dependences exhibit the decay of the film optical transmittance with an increase in the dose of absorbed photons. To obtain a unified basis for comparison of the transmission relaxation $T(t)/T_0$ curves, we used the so-called stretched exponential and single-exponential presentation for the relaxation curves in the form:

$$T(t)/T(0) = A_0 + A\exp[-(t-t_0)/\tau]^{(1-\beta)} \quad (5)$$

$$T(t)/T(0) = A_0 + A\exp[-(t-t_0)/\tau] \quad (6)$$

Here, t is the exposure time, τ is the apparent time constant, A characterizes the exponent amplitude, t_0 and A_0 are the initial coordinates, and α is the dispersion parameter ($0<\beta<1$).

For the obtained relaxation curves, a fairly wide scatter of parameters is observed for samples of the different composition. For doped samples, the cause of this dispersion may be that the concentration and distribution uniformity of impurity are not adequately preserved along the film during deposition. However, the relaxation curves are significantly different in the case of non-doped $As_4S_3Se_3$ as well. Comparison of the parameters of the relaxation curves for samples deposited at different incident angles has shown that, in the considered limits of distance from the center over the evaporator, the greatest effect of photodarkening is observed for the central samples, in contrast to the results reported in the literature for obliquely deposited films [12]. A slight decrease in the photodarkening amplitude with the distance from the center is due to a decrease in the film thickness.

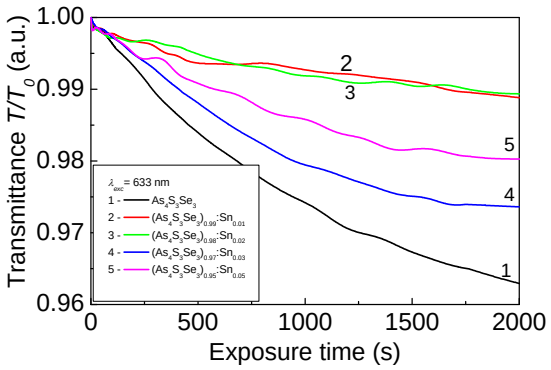

Fig. 5. Relaxation curves of photodarkening $T/T_0 = f(t)$ for amorphous $(As_4S_3Se_3)_{1-x}$:Sn_x thin films under light exposure at wavelength $\lambda = 633$ nm.

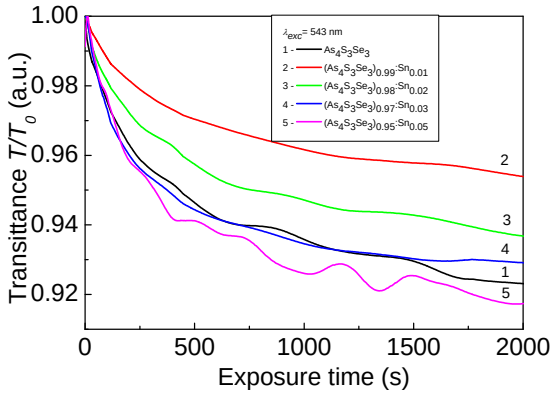

Fig. 6. Relaxation curves of photodarkening $T/T_0 = f(t)$ for amorphous $(As_4S_3Se_3)_{1-x}$:Sn_x thin films under light exposure at wavelength $\lambda = 543$ nm.

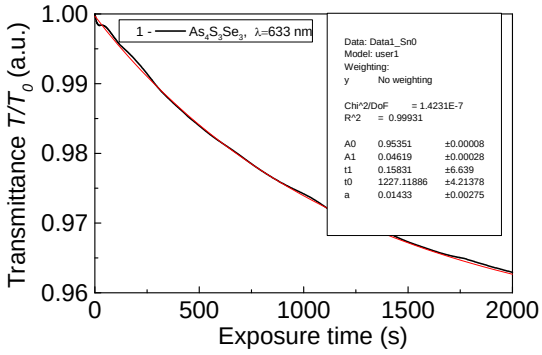

Fig. 7. Normalized optical transmittance kinetics for a He–Ne laser beam (λ = 633 nm) for amorphous $As_4S_3Se_3$ thin films.

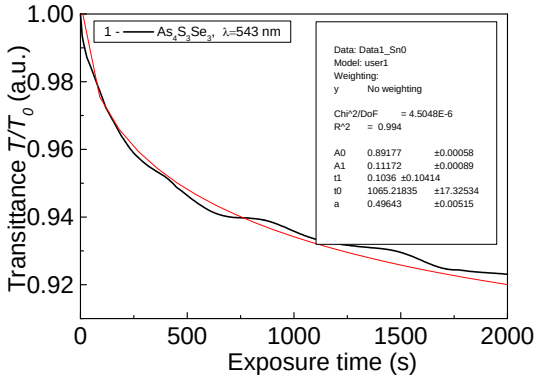

Fig. 8. Normalized optical transmittance kinetics for a He–Ne laser beam (λ = 543 nm) for amorphous $As_4S_3Se_3$ thin films.

The photodarkening phenomenon in chalcogenide glass films under illumination has no plain explanation up to now in spite of detailed investigation and a series of models advanced for interpretation of it. Several models have been put forward to substantiate this broadening

considering a particular individual atom as an initial object of photoexcitiation [13, 14]. Recently, a novel model for photodarkening in a-$As_2Se(S)_3$ has been proposed [15, 16], in which photoexcited charge carriers in extended states are considered to be responsible for photodarkening.

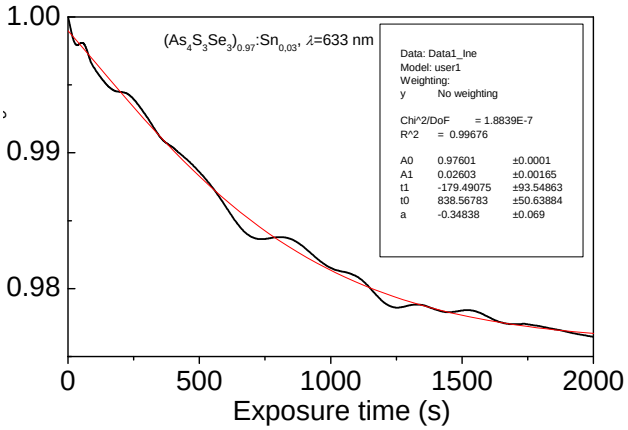

Fig. 9. Normalized optical transmittance kinetics for a He−Ne laser beam (λ = 633 nm) for amorphous $(As_4S_3Se_3)_{0.97}$:$Sn_{0.03}$ thin films.

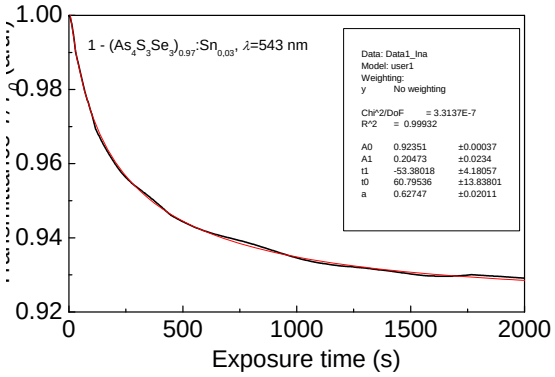

Fig. 10. Normalized optical transmittance kinetics for a He−Ne laser beam (λ = 543 nm) for amorphous $(As_4S_3Se_3)_{0.97}$:$Sn_{0.03}$ thin films.

Unlike the previous conceptions, the new model takes into account the layered cluster structure of a chalcogenide glass. During exposure, the layer is negatively charged due to capture of photoexcited electrons, and repulsive forces are built between the layers. These forces cause enlargement of the interlayer distance (leading to photoexpansion) and slip motion along the layers. The last-mentioned process alters the interaction of lone-pair electrons between the layers leading to a photodarkening effect. Earlier, in a structural model proposed for explanation of photodarkening phenomena, M. Popescu [17] has pointed out that distortion in the second and third coordination spheres should be taken into account as important factors.

The model of Shimakawa et al. [15, 16] offers a good basis for consideration of the effect on photodarkening of impurity atoms with coordination different from that of the host glass atoms, as in the case of tin. The foreign metal atoms provide bridging between the layers and hence reduce the slip motion, thus hindering the photodarkening. We suggest that this consideration is applicable in the case of tin impurity in amorphous $[(As_2S_3)_{0.5}$:$(As_2Se_3)_{0.5}]_{1-x}$:Sn_x thin films. Upon the addition of Sn, due to the tetrahedral arrangement of the sp^3 bonds with the chalcogens, the dopant atom inserted in the network increases the thickness of the layered configuration as revealed by the significant shift of the FSDP towards lower angles. This insertion corresponds in fact of introduction of the structural units of the $SnSe_2$ type in the network. The transition to a three-dimensionally (3D) network is preceded by the appearance of structural units of the SnSe type. Then, the direct consequence of this transition will be shown in the intensity of the FSDP which gradually disappears. The interruption of the two-dimensional structure and transition is probably due to a more ionic character of the Sn-Se bonds. Since tin tends to form directional bonds being introduced in the host glass and especially during annealing, some bridging bonds should appear between the layers. The structure of the glass that contains tin impurity requires therefore some excess slip forces; that is, it leads to greater

exposition doses and time constants.

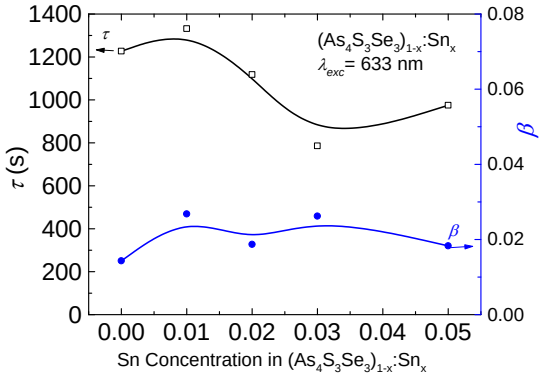

Fig. 11. Fitting parameters τ and β in equation (5) for the normalized optical transmittance kinetics for a He–Ne laser beam (λ = 633 nm) for amorphous $(As_4S_3Se_3)_{1-x}$:Sn_x thin films.

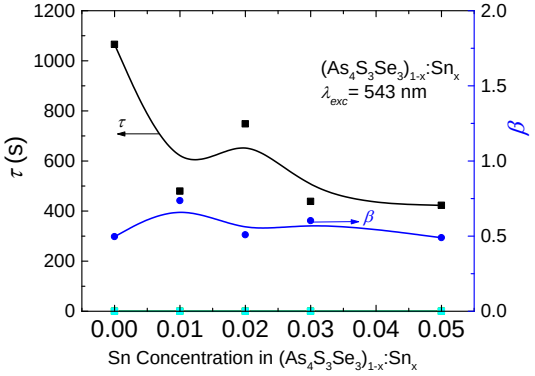

Fig. 12. Fitting parameters τ and β in equation (5) for the normalized optical transmittance kinetics for a He–Ne laser beam (λ = 543 nm) for amorphous $(As_4S_3Se_3)_{1-x}$:Sn_x thin films.

The stretched exponential photodarkening kinetics was numerically justified for thick amorphous As-Se films [18, 19]. It was shown that in-situ photodarkening kinetics are quite similar in amorphous $As_{40}Se_{60}$ and $As_{50}Se_{50}$ films and exhibit a strong tendency to non-dispersion (β values from equation (1) are slightly deviated around 0.6, while photodarkening in $As_{60}Se_{40}$ films mainly corresponds to single-exponential rule with β value close to 1.0). It was also established that the parameter β values depend on the thickness of the sample. If the film thickness is smaller than the penetration depth of the excitation light, the dispersion parameter β = 1, which indicates that the photodarkening kinetics can be presented by an exponential function (equation (6)). In our case, the penetration depth is defined by the excitation wavelength. It is evident that the penetration depth is higher if the amorphous film is excited at a longer wavelength (λ = 633 nm) than in the case of a shorter wavelength (λ = 543 nm).

The parameters τ and β from equations (5) and (6) were calculated by the computer fitting of the normalized optical transmittance kinetics curves for exposure of amorphous $(As_4S_3Se_3)_{1-x}$:Sn_x thin films to a He–Ne laser beam (λ = 633 and 543 nm). Figures 11 and 12 represent the fitting parameters τ and β according to equation (5) versus Sn concentration in amorphous $(As_4S_3Se_3)_{1-x}$:Sn_x thin films. We obtain that, if the thin amorphous film is excited at a longer wavelength (λ = 633 nm), the values of the dispersion parameter β are smaller, which means that dispersion is more pronounced.

The fact that the photodarkening kinetics may be described by a stretched exponential can be regarded as an indication of dispersion by a kinetic mechanism, i.e., the time dependence of the process rate [20]. The data allow concluding that the formation of photoinduced absorption is limited to a dispersive process with the exponent $\beta \cong 0.5$. Charge transport in chalcogenide glasses is known as highly dispersive due to wide distribution of capture times in multiple-trapping process [21]. For a-As_2Se_3-like glasses, the dispersive parameter β of hole transport is close to 0.5, in accordance with the value found from the stretched exponential presentation of photodarkening kinetics [9].

The transmission hologram gratings in amorphous $(As_4S_3Se_3)_{1-x}$:Sn_x thin films with a period Λ = 1μm were recorded by two symmetrically incident Ar^+ laser beams (DPSS-laser) of

equal intensity (λ = 532 нм), and the readout of the diffraction efficiency η was made using a diode laser beam (λ = 650 нм) in the first diffraction maximum.

The optical set-up is illustrated in Fig. 13. Diffraction efficiency η was defined as $\eta = \frac{I_d}{I_0}$, where I_0 is the intensity of the readout beam and I_d is the intensity of the first order diffracted beam. Figure 14 represents the growth of diffraction efficiency $\eta(t)$ during the registration of elementary microhologram in amorphous $(As_4S_3Se_3)_{1-x}$:Sn_x thin films. The kinetics of diffraction efficiency growth $\eta(t)$ was measured by registration of the laser intensity of the 1st interference maximum versus time exposure. With an increase in the Sn concentration in amorphous $(As_4S_3Se_3)_{1-x}$:Sn_x thin films up to 6.0 at % Sn, diffraction efficiency η increases, while for higher concentrations of tin, it decreases (Fig. 15.)

The dependence of the diffraction efficiency versus thin film thickness (L = 0.88−17.5 μm) was also investigated. Figure 16 represents the kinetics of the registration process of the gratings $\eta(t)$ for amorphous $As_4S_3Se_3$ thin films with different thickness. For amorphous $As_4S_3Se_3$ thin films, it was demonstrated that the maximum of diffraction efficiency η is obtained for the films with a thickness of about L = 4.0 μm. A similar dependence was previously obtained for amorphous $As_{40}S_{60}$ and $As_{55}Se_{45}$ thin films [22, 23]. The dependence of photodarkening for as-evaporated amorphous As-Se [24] and As_2Se_3:Pr(Dy) thin films was also found [25].

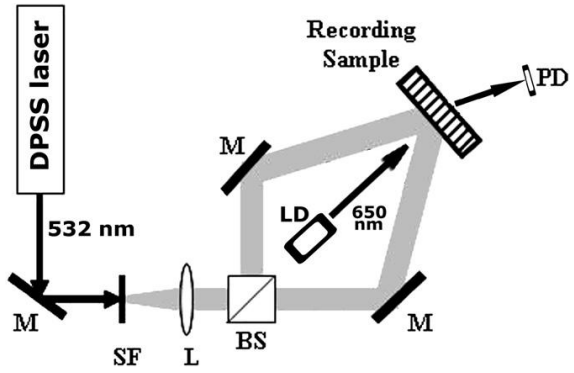

Fig. 13. Experimental set-up for Bragg grating recording in chalcogenide amorphous thin films: DPSS-laser (λ = 532 нм, 30 mW/cm^2), M-mirror, SF-spatial filter, L-lens, BS-beam splitter, LD-laser diode (λ = 650 нм), PD-photodiode.

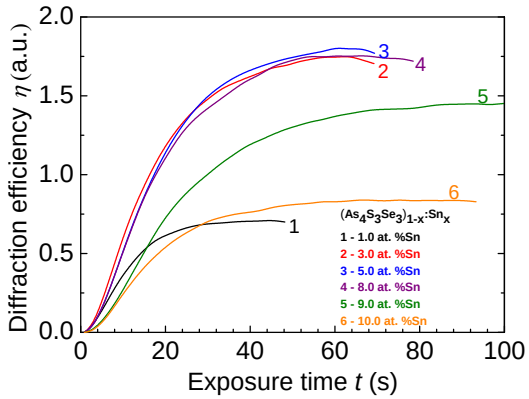

Fig. 14. Kinetics of diffraction efficiency $\eta(t)$ for different compositions of amorphous $(As_4S_3Se_3)_{1-x}$:Sn_x thin films.

The dependence of the photodarkening amplitude on the thickness of the amorphous thin film is due mainly to the dependence of the position of optical absorption edge, which regulates the amount of absorbed photons generating the photodarkening process. As in our case, for amorphous As_2S_3 [22] and As_3Se_2 [24] thin films, the diffraction efficiency and the photodarkening effect were achieved for the thickness of the amorphous film of about L = 4.0 μm. In addition to the thickness dependence of the position of the optical absorption edge, the thickness dependence of the photodarkening in amorphous As_2S_3 thin films was also explained by the strain induced by the lattice mismatch between the film and the substrate [26].

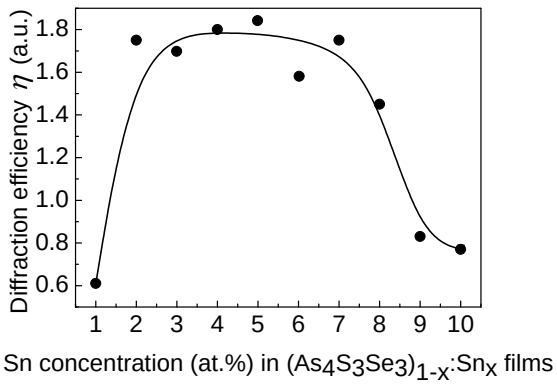

Fig. 15. Dependence of diffraction efficiency η versus Sn concentration in amorphous $(As_4S_3Se_3)_{1-x}:Sn_x$ thin films.

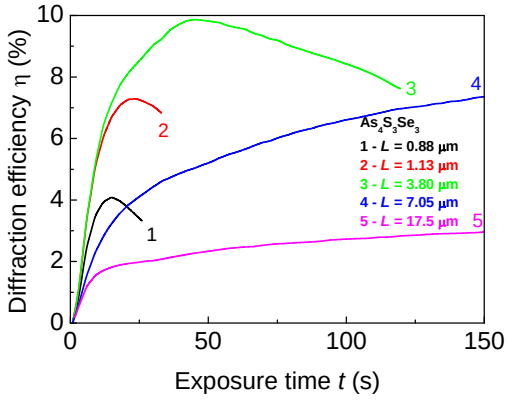

Fig. 16. Kinetics of diffraction efficiency $\eta(t)$ for amorphous $As_4S_3Se_3$ thin films with different thickness.

The thickness dependence of the photodarkening kinetics of optical transmittance in amorphous As-Se films also was interpreted on the basis of change in the penetration depth of the incident laser beam during exposure [18, 19]. It was shown that the photostructure transformations in an amorphous film depend on the thickness of the amorphous film and are fairly complicated depending on the nature of evolving changes in short- and long-range ordering near-neighbor interactions in the disordered lattice.

4. Conclusions

The experimental results of steady-state photoconductivity, relaxation of photodarkening and holographic characteristics of amorphous $(As_4S_3Se_3)_{1-x}:Sn_x$ thin films are described. It is shown that the photoconductivity spectra depend on the polarity on the top illuminated electrode and on the Sn concentration in the host glass. The photosensitivity of amorphous $(As_4S_3Se_3)_{1-x}:Sn_x$ thin films is almost constant for all Sn-containing glasses. The Moss rule is used for determination of optical forbidden gap E_g from the photoconductivity spectra. It is demonstrated that the investigated amorphous films are sensitive to light irradiation and can be used as effective registration media for holographic information. The relaxation of photodarkening in amorphous $(As_4S_3Se_3)_{1-x}:Sn_x$ thin films is investigated; it is shown that the relaxation curves of transmittance $T/T_0 = f(t)$ can be described the stretched exponential function $T(t)/T(0) = A_0+A\exp[-(t-t_0)/\tau]^{(1-\beta)}$. Diffraction efficiency η measured in the 1st interference maximum in amorphous $(As_4S_3Se_3)_{1-x}:Sn_x$ thin films increases upon doping with tin up to 6.0 at % Sn.

Acknowledgments. This work was supported by the SCSTD of the Academy of Sciences of Moldova, project no. 11.817.05.03A.

References

[1] M. Popescu, A. Andriesh, V. Ciumash, M. Iovu, S. Shutov, and D. Tsiuleanu, Physics of chalcogenide glasses, Editura Ştiinţifică Bucureşti – I.E.P. Ştiinţa Chişinău, 1996.

[2] O. V. Iaseniuc, D. V. Harea, M. S. Iovu, E. P. Colomeico, E. E. Harea, I. A. Cojocaru, D. F. Shepel, and A. Meshalkin, Spectroscopic study of amorphous As_2Se_3:Sn_x and $(As_2S_{1.5}Se_{1.5})_{1-x}$:$Sn_x$ thin films, Proc. SPIE 8411, Advanced Topics in Optoelectronics, Microelectronics, and Nanotechnologies VI, 8411OL (November 1, 2012).

[3] O. V. Iaseniuc, D. V. Harea, E. E. Harea, G. F. Volodina, and M. S. Iovu, Mold. J. Phys. Sci. 12(3-4), 181 (2013).

[4] A. V. Stronski, M. Vlcek, S. A. Kostyukevych, V. M. Tomchuk, E. V. Kostyukevych, S. V. Svechnikov, A. A. Kudreavtsev, N. L. Moskalenko, and A. A. Koptyukh, Sem. Phys., Quantum Electron. Optoelectron. 5(3), 284 (2002).

[5] M. Reinfelde, and J. Teteris, J. Optoelectron. Adv. Mater. 13(11-12), 1531 (2011).

[6] M. S. Iovu, S. D. Shutov, and L. Toth, Physica Status Solidi (b), 195, 149 (1996).

[7] M. S. Iovu, N. N. Syrbu, S. D. Shutov, I. A. Vasiliev, S. Z. Rebeja, E. P. Colomeico, M. Popescu, and F. Sava, Physica Status Solidi (a), 175(2), 623 (1999).

[8] M. S. Iovu, S. D. Shutov, V. I. Arkhipov, and G. J. Adriaenssens, J. Non-Cryst. Solids 299&302, 1008 (2002).

[9] P. Boolchand, D. G. Georgiev, and M. S. Iovu, Chalcogen. Lett. 2(4), 27 (2005).

[10] M. S. Iovu, D. V. Harea, I. A. Cojocaru, E. P. Colomeico, A. M. Prisacari, and V. G. Ciorba, J. Optoelectron. Adv. Mater. 9(10), 3138 (2007).

[11] G. Moddel, D. A. Anderson, Poyl, W., Phys. Rev. B22, 1918 (1980).

[12] Y. Kuzukawa, A. Ganjoo, and K. Shimakawa, Phil. Mag. B79(2), 249 (1999).

[13] G. Pfeiffer, M. A. Paesler, S. C. Agarwal, J. Non-Cryst. Solids, 130, 111 (1991)

[14] K. Shimakawa, A. Kolobov, and S. R. Elliot, Adv. Phys. 44, 775 (1995).

[15] K. Shimakawa, N. Yoshida, A. Ganjoo, Y. Kuzukawa, and J. Singh, Phil. Mag. Lett., 77**,** 153 (1998).

[16] A. Ganjoo, N. Yoshida, and K. Shimakawa, Photoinduced changes on the structural and electronic properties of amorphous semiconductors, Recent Research Developments in Applied Physics, ed. M.Kawasaki, N. Ashgritz and R. Anthony (Research Signpost, Trivandrum, 2, 129-150 (1999).

[17] M. Popescu, J. Non-Cryst. Solids, 90(1-3), 533 (1987).

[18] V. O. Balitska, M. S. Iovu, and O. I. Shpotyuk, J. Optoelectron. Adv. Mater. 14(7), 590 (2012).

[19] V. O. Balitska, M. S. Iovu, and O. I. Shpotyuk, J. Non-Cryst. Solids, 379, 182 (2013).

[20] D. L. Gisom, M. T. Gingerich, E. J. Frieble, Phys. Rev. Lett., 71, 1019 (1993).

[21] G. Pfister, and H. Sher, Adv. Phys. 27(5), 747 (1978).

[22] J. J. Teteris, Optoelectron. Adv. Mater. 4(3), 687 (2002).

[23] J. Teteris, and M. Reinfelde, J. Optoelectron. Adv. Mater. 7(5), 2581 (2005).

[24] M. S. Iovu, V. G. Ciorba, E. P. Colomeico, M. A. Iovu, A. M. Nastas, A. Prisacari, M. Popescu, and O. I. Shpotyuk, J. Optoelectron. Adv. Mater. 7(5), 2333 (2005).

[25] M. S. Iovu, S. D. Shutov, P. Boolchand, E. P. Colomeico, V. G. Ciorba, S. M. Iovu, and M. Popescu, J. Optoelectron. Adv. Mater. 4(4), 857 (2002).

[26] K. Hayashi, and N. Mitsuishi, J. Non-Cryst. Solids 299&302, 949 (2002).